Hindawi
Geofluids
Volume 2023, Article ID 9311206, 14 pages
https://doi.org/10.1155/2023/9311206

Research Article

Experiment and Numerical Simulation of Strength and Stress Distribution Behaviors of Anchored Rock Mass in a Roadway

Honghui Zhao,[1,2] Haijian Su ,[1] Xiaofeng Qin,[1] Kai Zhang ,[1] Yu Jiang,[1] and Wenbo Wang[1]

[1]*State Key Laboratory for Geomechanics and Deep Underground Engineering, China University of Mining and Technology, Xuzhou 221116, China*
[2]*East China Environmental and Geotechnical Engineering Branch, China National Petroleum Corporation, Qingdao 266000, China*

Correspondence should be addressed to Haijian Su; hjsu@cumt.edu.cn

Received 24 February 2022; Revised 31 May 2022; Accepted 24 November 2022; Published 12 April 2023

Academic Editor: Chao-Zhong Qin

Due to the influence of the ground stress, mining disturbance, and other factors, the roadway surrounding rock in deep underground engineering such as mines, tunnels, and underground caverns is prone to looseness and deformation with the excavation of roadways. In such engineering, the bolt support is frequently employed to stabilize the surrounding rock. In this work, a part of the anchor and the surrounding rock were taken as a simplified model of the anchorage rock mass, and the laboratory compression test was performed on the similitude model. Then, the FLAC3D software was used to simulate varying numbers of bolts and different lateral pressure conditions, and the peak stress, the maximum principal stress field, and the anchor stress field distribution of the anchorage rock mass were obtained. The influence of bolt pretightening force and row spacing on the stability of surrounding rock was discussed using the combined arch theory. The results show that increasing the number of bolts and lateral pressure in the anchorage rock mass can significantly improve the stress value and distribution range of the maximum principal stress field and the anchorage stress field. The fluctuation of the anchorage stress field at different anchorage distances can be lessened by increasing the number of bolts (bolt density). When the lateral pressure exceeds 3 MPa, the anchorage mechanical characteristics of the anchorage rock mass tend to remain stable. The coverage of the effective anchorage stress field and the thickness of the surrounding rock anchorage composite arch can be increased by increasing the bolt pretightening force and decreasing row spacing, consequently improving the anchorage mechanical characteristics of the anchorage rock mass. The research results can be used as a theoretical reference for choosing appropriate bolt support parameters for the roadway surrounding rock.

1. Introduction

The surrounding rock of the roadway in deep engineering such as mines, tunnels, and underground caverns is prone to deformation due to the high ground stress, mining disturbance, and other factors [1, 2]. The excessive deformation of the surrounding rock structure may cause the floor heave, rib spalling, roof leakage, roof fall, and other phenomena [3–5], which manifests as the formation of a loose fracture structure with fully developed fractures in the rock mass around the roadway [6]. To ensure that roadways can be used normally, timely support is required from the start of excavation to limit deformation and displacement of the surrounding rock. It is critical to effectively strengthen the bearing capacity of the surrounding rock structure and the stability of the surrounding rock after support.

Bolt support, the most commonly used support measure in rock engineering, may effectively stabilize the surrounding rock by improving and making full use of the bearing capacity of the rock mass. Currently, research on bolt support can be roughly divided into three categories according to the main focus: (i) study on the effects of the properties of the anchored rock mass (surrounding rock), such as the lithology of the surrounding rock, the strength of the surrounding rock, joints, cracks, and weak interlayer [7–10]; (ii) study on the effects of external load, that is, considering the stress state (tension, compression, shear), loading, unloading, and the creep of the bolt according to the engineering site [11, 12]; (iii) study on the effects of the nature of the bolt itself, such as type, size (diameter, length), row spacing, pretightening force, and the spatial distribution position of multiple bolts [13–18]. Some contributed results have been obtained: in terms of the bolting mechanisms, Kang [19, 20] considered that the main function of bolt support on surrounding rock is to control the separation, sliding, cracking, and dilatancy deformation of rock mass in the anchorage zone and put forward the corresponding key bearing ring theory. Cao et al. [21] investigated the load transfer mechanism of the bolt support system, deduced the two-stage failure mode of the bolt anchorage system, and discussed the failure mode of the bolt by using a bond strength model and the iterative method. Song and Mu [22] discussed the theoretical calculation of the bearing capacity and supporting load of the bolt combination arch, the reasonable thickness of the combined arch, and the reasonable length of the anchor bolt and put forward relevant reasonable calculation formulas, based on the analysis of bolt-shotcrete support mechanism and failure characteristics of soft rock. In terms of anchorage mechanical properties, Guo et al. [23] established the mechanical model (considering the tray effect) of anchorage surrounding rock based on the elastic theory, believing that the influence of the tray on the stress of the surrounding rock supported by the bolt axis can be ignored except near the surface of the surrounding rock. Based on the self-developed test system of the composite bolt-rock bearing structures, Zhang et al. [24] investigated the influence of bolt support density on the bearing characteristics of anchor composite bearings, obtained the strength and failure characteristics of anchor composite bearings, and found the variation law of central stress and surrounding rock displacement of the composite bolt-rock bearing structure. Zong et al. [25] found that the number of bolts and the pretightening force would affect the failure mode. The failure mode of fractured sandstone changes from the tensile failure to tensile-shear mixed failure with the increase in bolts. The pretightening force can inhibit the formation and evolution of the tensile crack, delay the failure process of fractured sandstone under anchorage, and promote its transformation from the brittle failure to plastic failure. Du et al. [26] studied the effect of bolts on the stress redistribution of roadway surrounding rock and believed that the bolt could improve the strength of the roadway by increasing the minimum main force around the roadway. A comprehensive ground arch that is crucial to the stability of the roadway will be formed around the roadway under appropriate supporting conditions.

With the excavation of the roadway, the stress environment of the surrounding rock changes, and the plastic zone forms in the surrounding rock of the roadway. The stress is redistributed, and large stress appears in the roadway side area, which often causes the two sides to break and swell. The role of the bolt support is to keep the broken rock mass from separating, sliding, cracking, and deforming. Therefore, this work took the bolt support of the roadway surrounding rock in Gubei coal mine as the background. The surrounding rock of the roadway sidewall area under the anchorage effect of the bolt was taken as the research area (Figure 1), which was simplified as the model of the anchorage rock mass. Laboratory tests and FLAC3D numerical simulation tests were carried out to study the mechanical properties of the surrounding rock anchorage under varied bolt numbers (bolt density) and different lateral pressures. In addition, the influence of bolt pretightening force and bolt row spacing on the anchorage effect of the surrounding rock was discussed based on the combined arch theory.

2. Experimental Study of Anchorage Effect of Surrounding Rock Mass

2.1. Experimental Method and Procedure. A similitude model was poured according to the real mechanical properties of the surrounding rock mass in the Gubei coal mine, Huainan mining area, China. To simulate the anchorage rock mass in line with the actual state of the site to a large extent, the aggregate of the pouring model (the aggregate gradation was 8~10 cm) was picked from the rock of the actual roadway site in the test process. Quartz sand, cement, and gypsum combined with a certain amount of water were selected as the anchorage rock mass model cementing materials. Through many comparative tests, the mass ratio of the quartz sand, cement, gypsum, and water was chosen as 0.5 : 1 : 0.2 : 0.6. The size of the rock specimen is frequently chosen as large as feasible in the rock mechanics tests using a physical similarity model, and the ideal state is to construct a model that is close to the real size, because the larger the rock sample size, the more accurately the test findings can reflect the actual engineering properties. However, the test devices and other factors limit the size of the specimen. After careful consideration of the above issues, the actual anchored surrounding rock mass was adequately simplified. The cubic anchorage rock mass specimen with a size of 200 mm* 200 mm* 200 mm was poured in this work utilizing the above ingredients and ratios, as indicated in Figure 2(a) [27, 28]. After pouring in the mold, the specimen was left for 24 hours in its natural state and then removed. Then, the specimen was put into the maintenance water tank at a constant temperature for 7 days and, finally, made it naturally air dried and wrapped with preservative film to maintain moisture content. At the same time, the specimens without bolt reinforcement were also prepared for comparative analysis.

The anchor bolt was placed after the anchorage rock specimen was poured, as shown in Figure 2(b). First, a 12 mm diameter prefabricated bolt hole was bored in the center of the specimen. Then, the bolt was mounted, as illustrated in Figure 2(c), with bolts, pallets, nuts, and gaskets as its primary components. A torsion wrench was used to apply a pretightening force of 15.59 kN to the bolt. The 7075-T6 aluminum alloy rod with a diameter of 10 mm was chosen to simulate the body of the anchor bolt. To determine the mechanical properties of the anchor bolt, a tensile test of the aluminum alloy metal rod was performed prior to the

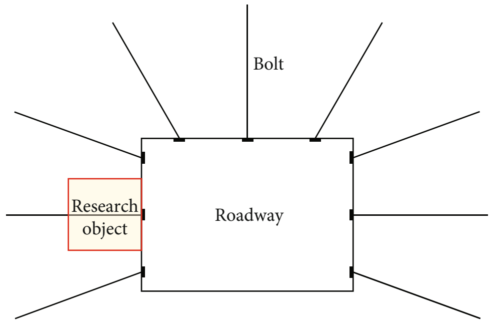

Figure 1: Research object of surrounding rock mass in a roadway.

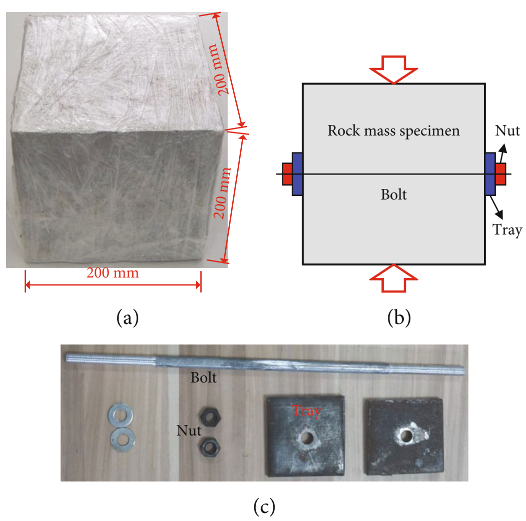

Figure 2: (a) Rock mass specimen, (b) schematic diagram of anchorage method, and (c) bolt and auxiliary appliances.

start of the test. The elastic modulus, yield strength, yield strain, and peak stress of the aluminum alloy metal rod were 70.65 GPa, 426.59 MPa, $7.69^{*}10^{-3}$, and 559.9 MPa, respectively. The tray was a square steel plate with a size of 70 mm*70 mm*10 mm and a middle hole diameter of 12 mm.

The YNS2000 servo test system, with a maximum test force of 2000 kN, was used to perform the compression tests. During the loading operation, the test system will automatically collect data on the axial displacement and axial force of the loaded specimen. In the test, a loading rate of 0.5 mm/min was used. Before the test, a reasonable amount of Vaseline was evenly placed over the upper and lower ends of the specimen to reduce the influence of end-face friction on the test findings.

2.2. Experimental Result and Analysis. Figure 3 shows the axial stress-strain curves of the anchored and unanchored rock mass model specimens. The compaction stage (*oa*), the linear elastic growth stage (*ab*), the plastic deformation stage (*bc*), and the strain softening stage (*cd*) are all found in the axial loading curves of the two models, according to the test results. The peak strength and elastic modulus of the specimen after anchorage have increased by 36.65% and 28.33%, respectively, from 9.25 MPa and 1.20 GPa to 12.64 MPa and 1.54 GPa. Furthermore, following anchorage, the residual strength of the surrounding rock model specimen is much higher than that before anchorage.

Three states (the initial failure state, axial stress peak state, and final state) of the specimen were chosen to compare the failure characteristics of the anchored and unanchored rock mass model specimens, as shown in Figure 4. Compared with the anchored, the broking degree of the unanchored surrounding rock model sample is relatively lower. The number of cracks propagating on the surface of the specimen is noticeably lower at the peak state and final state, and the specimen is eventually destroyed by multiple massive cracks. When the anchorage surrounding rock model specimen ultimately breaks, many cracks appear inside the specimen, and the degree of fracture is substantially greater than that of the model specimen without anchorage. In summary, the surrounding rock interacts with the bolt to generate an anchorage rock mass under the action of bolt support. The bolt has strong supporting ability, which can effectively improve the bearing capacity of the surrounding rock while reducing deformation and failure [29, 30].

3. Numerical Simulation of Anchorage Mechanical Properties of Surrounding Rock Mass

3.1. Establishment of the Numerical Model. The numerical calculation method has been widely and rapidly applied in the study of geotechnical engineering problems with the rapid development of computer technology, which tremendously promotes the development of geotechnical mechanics. It is becoming increasingly significant in numerous domains of modern science and technology due to its remarkable benefits of high reproducibility, fast cycle time, and low cost. FLAC3D is a three-dimensional fast Lagrangian analysis program developed by Itasca in the United States that can better simulate the mechanical behavior of geological materials when reaching the strength or yield limit and makes complex geotechnical engineering or mechanical problems easy to simulate [31, 32]. Due to the influence of test conditions and other factors, it is difficult to obtain the distribution characteristics of parameters such as the stress field in the physical model. Therefore, this work used the FLAC3D numerical software to study and analyze the surrounding rock anchorage model.

As shown in Figure 5, the FLAC3D numerical model was built as a cube with a side length of 200 mm, which mainly includes the model body, anchor bolt, and tray (70 mm*70 mm*10 mm) based on the physical model test of the surrounding rock anchorage. The center of the model was symmetrically arranged and positioned at the origin of the coordinates. The model contained 64784 units and 70271 nodes after meshing. To better understand the interaction mechanism between nearby bolts, the internal stress distribution of the anchorage model was obtained by numerical model experiments with various bolt densities. On the basis of controlling the tray size of the model, five numerical simulation models with anchor density of 0, 1, 2, 3, and 4 are established. As illustrated in Figure 5(a), each bolt was

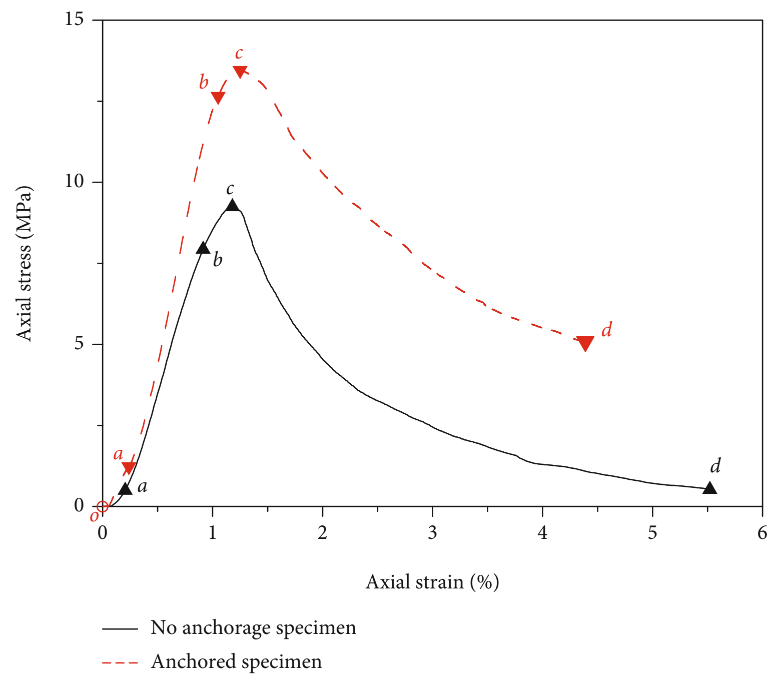

Figure 3: Axial stress vs. axial strain curve of rock mass specimen under uniaxial compression.

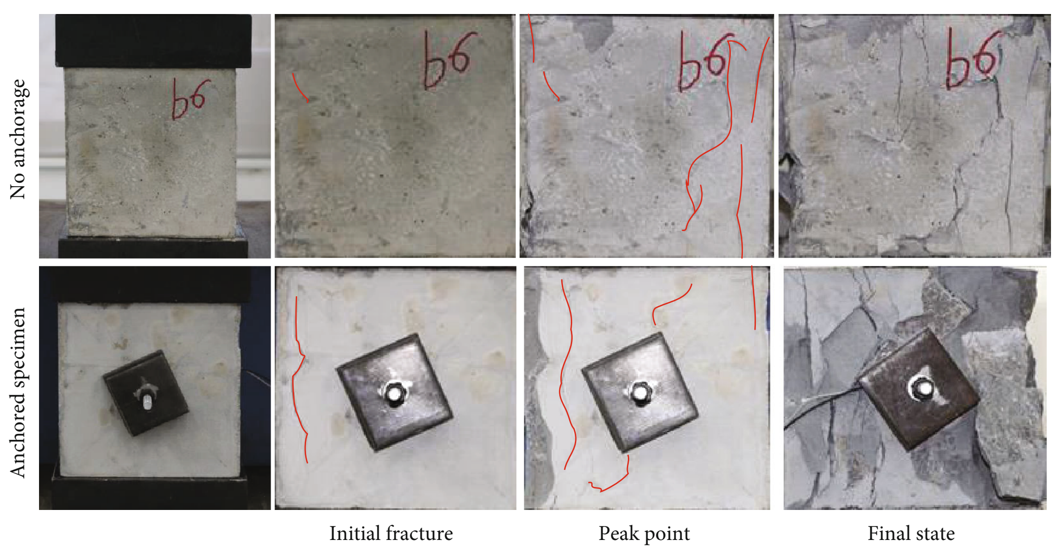

Figure 4: Fracture process of rock mass specimen during uniaxial compression.

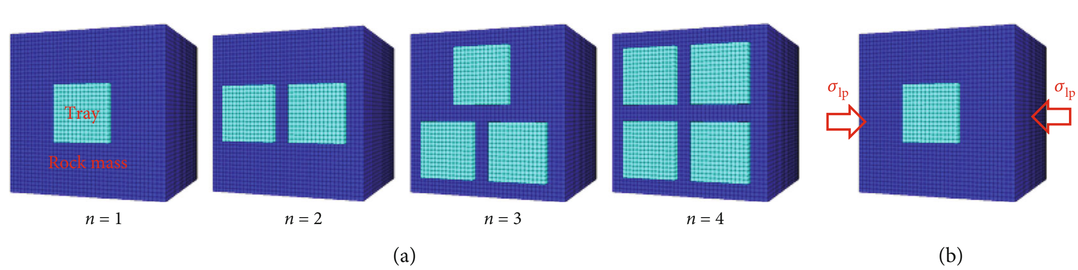

Figure 5: Numerical simulation mode of rock mass specimen with different (a) bolt number and (b) lateral pressure, respectively.

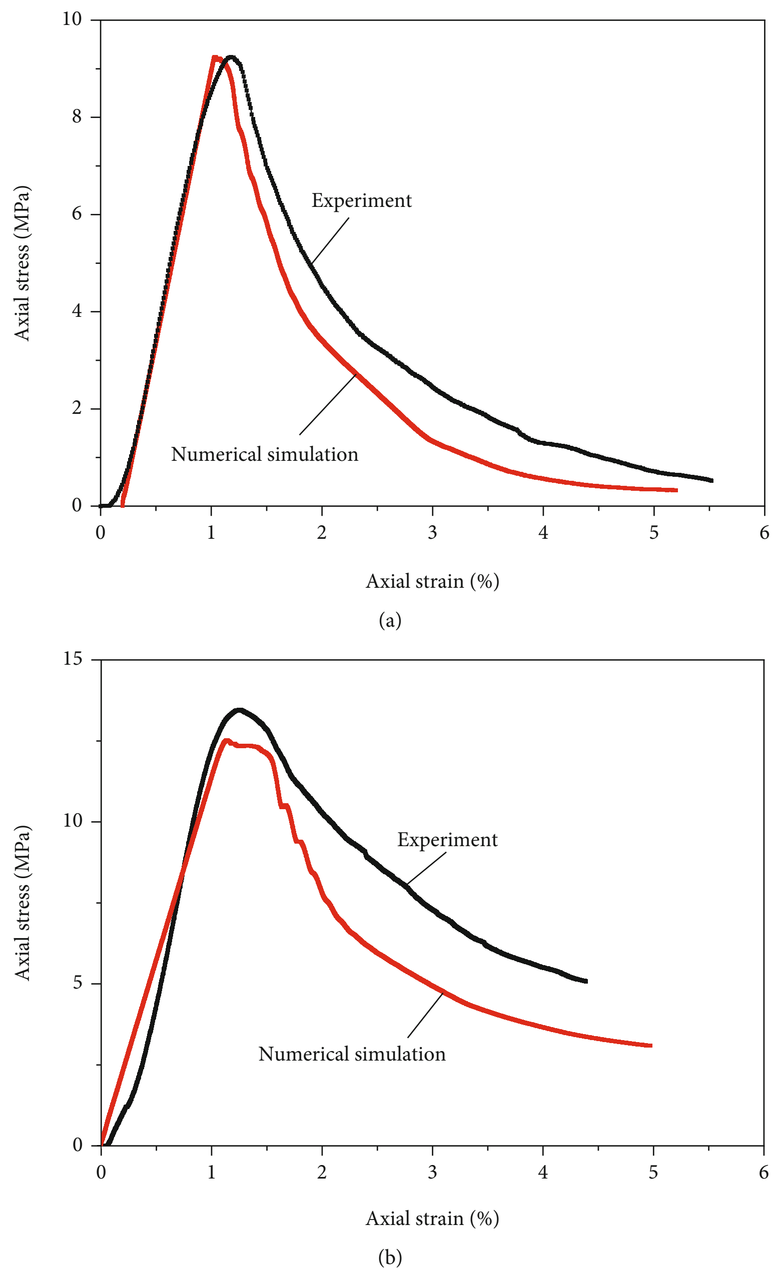

Figure 6: Axial stress vs. axial strain curve comparison between experiment and numerical simulation results of rock mass specimen with (a) no bolt and (b) one bolt reinforced, respectively.

preloaded at 15 kN. The front and back sides of the model were configured as free surfaces (vertical x direction), and varied lateral pressure could be added to the simulation to simulate the lateral restricting pressure of the actual surrounding rock mass. As indicated in Figure 5(b), the left and right sides of the model were anchorage surfaces (vertical y direction), whereas the upper and bottom sides were displacement loading surfaces (vertical z direction). The quantitative test findings revealed that when deformation increased in the post-peak loading stage, the mechanical properties of rock materials deteriorated gradually, exhibiting strain softening characteristics, which was consistent with the physical model test results in Section 2.2. Therefore, combined with the characteristics of the constitutive relations in the numerical simulation software, the strain softening constitutive relation was picked for the simulation calculation. The selection of the basic mechanical parameters of the model: the prepeak linear elastic stage parameters of the model were determined by the previous laboratory physical model test. The postpeak strain softening parameters of the model were investigated by comparing the stress-strain curves of the physical model with those determined by the inversion method. As illustrated in Figure 6, the axial stress-strain curves of the specimens of unanchored and anchored with a single anchor obtained through numerical simulation were compared to those acquired from the physical model test in Section 2.2. The peak strength and elastic modulus of the unanchored model were 9.25 MPa, 1.20 GPa (laboratory test results) and 9.25 MPa, 1.19 GPa

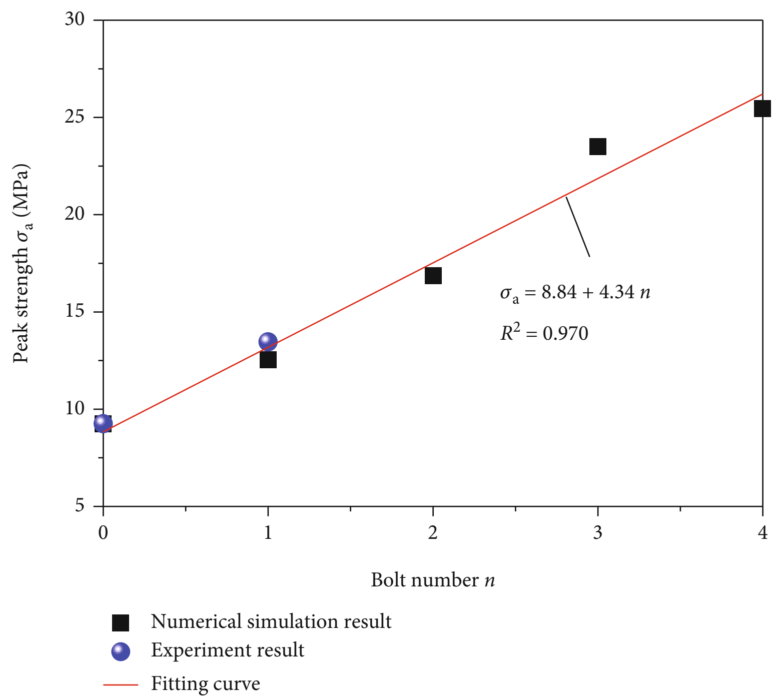

Figure 7: Relationship between peak strength and bolt number of rock mass specimen.

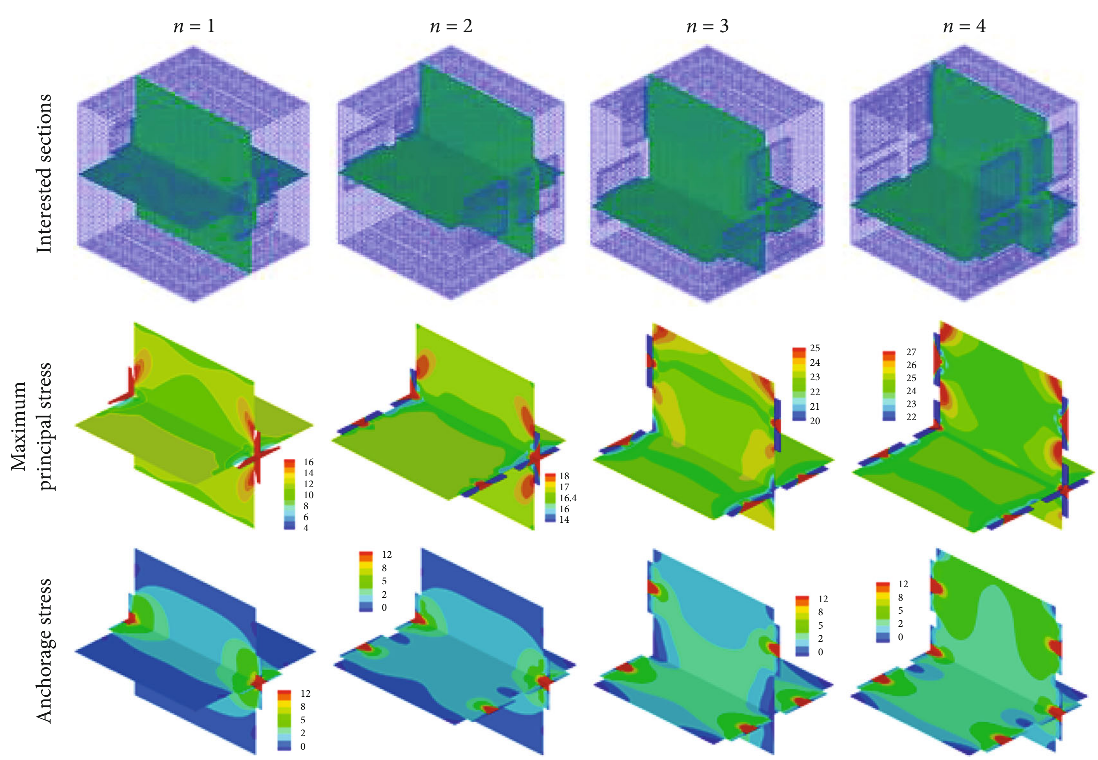

Figure 8: Maximum principal stress and anchorage stress distributions of rock mass specimen with different bolt numbers.

(numerical simulation results), respectively, and the values after anchorage were 12.64 MPa, 1.54 GPa (laboratory test results) and 12.53 MPa, 1.51 GPa (numerical simulation results), respectively. The fitting degree of the surrounding rock mass model's axial stress-strain curve was high in both the prepeak and postpeak stages, regardless of whether the surrounding rock was anchored or not, implying that the selected model's postpeak strain softening parameters were well in line with the test requirements, ensuring the reliability of the subsequent test results.

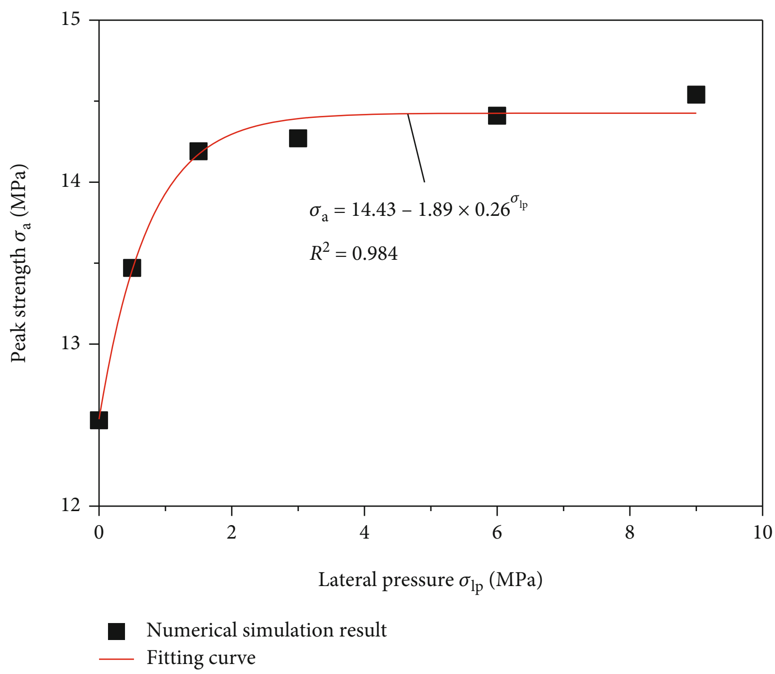

FIGURE 9: Relationship between peak strength and lateral pressure of rock mass specimen.

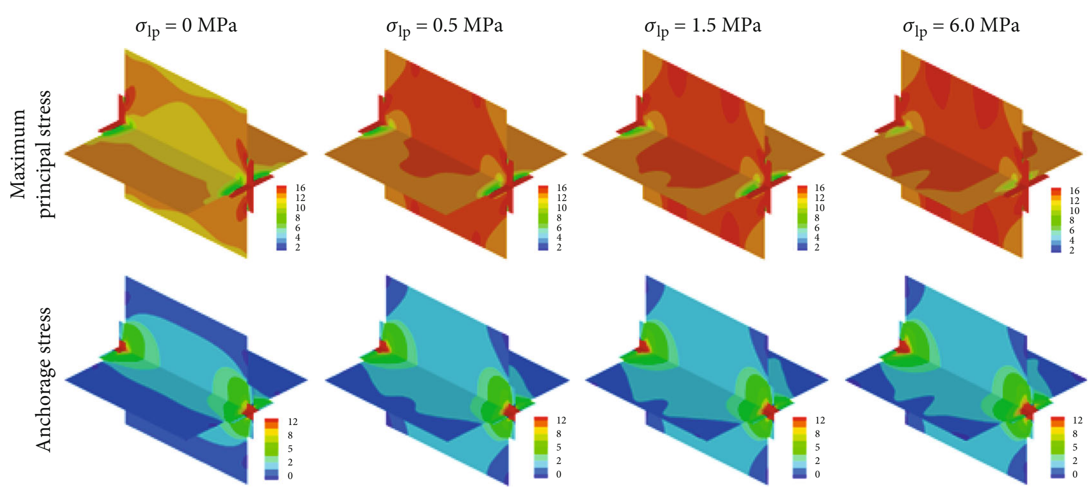

FIGURE 10: Maximum principal stress and anchorage stress distributions of rock mass specimen with different lateral pressures.

3.2. Influence of Bolt Number on the Mechanical Behaviors of Rock Mass. According to the axial peak strength of specimens under different bolt numbers calculated by numerical simulation, the relationship between axial peak strength and the bolt number was obtained, as shown in Figure 7. It can be seen that the peak strength and bolt number show a significant positive linear relationship. As the bolt number changes from 0 to 1, the peak strength of the model rises from 9.25 MPa to 12.53 MPa, with a change extent of 35.46%. As the bolt number increases, the axial peak strength of the surrounding rock anchorage model sample gradually rises. In the bolt number range of 0~3, the axial peak strength of the model sample increases by about 36.49%. When the bolt number increases from 3 to 4, the increasing rate is 8.29% of the axial peak strength, and the increasing rate decreases significantly. It can be discovered that a reasonable density of the bolt provides the optimal stability control effect on the rock mass.

Figure 8 depicts the model's internal maximum primary stress field at peak time as well as the anchorage stress field. The maximum primary stress, which was commonly stated as the vector sum of normal and shear stresses, was a widely used metric for assessing the stability of a structure's interior parts. Two mutually perpendicular planes were selected as monitoring planes in the model to explore the stress features of internal space and the action mechanism of the bolt with varying bolt numbers in the loading process of the anchorage surrounding rock mass model. For the single bolt anchorage surrounding the rock mass model, there was a noticeable stress rise zone from the connection between the bolt and the tray along the *z* direction of compression to the inclined direction of the two loading ends. In the

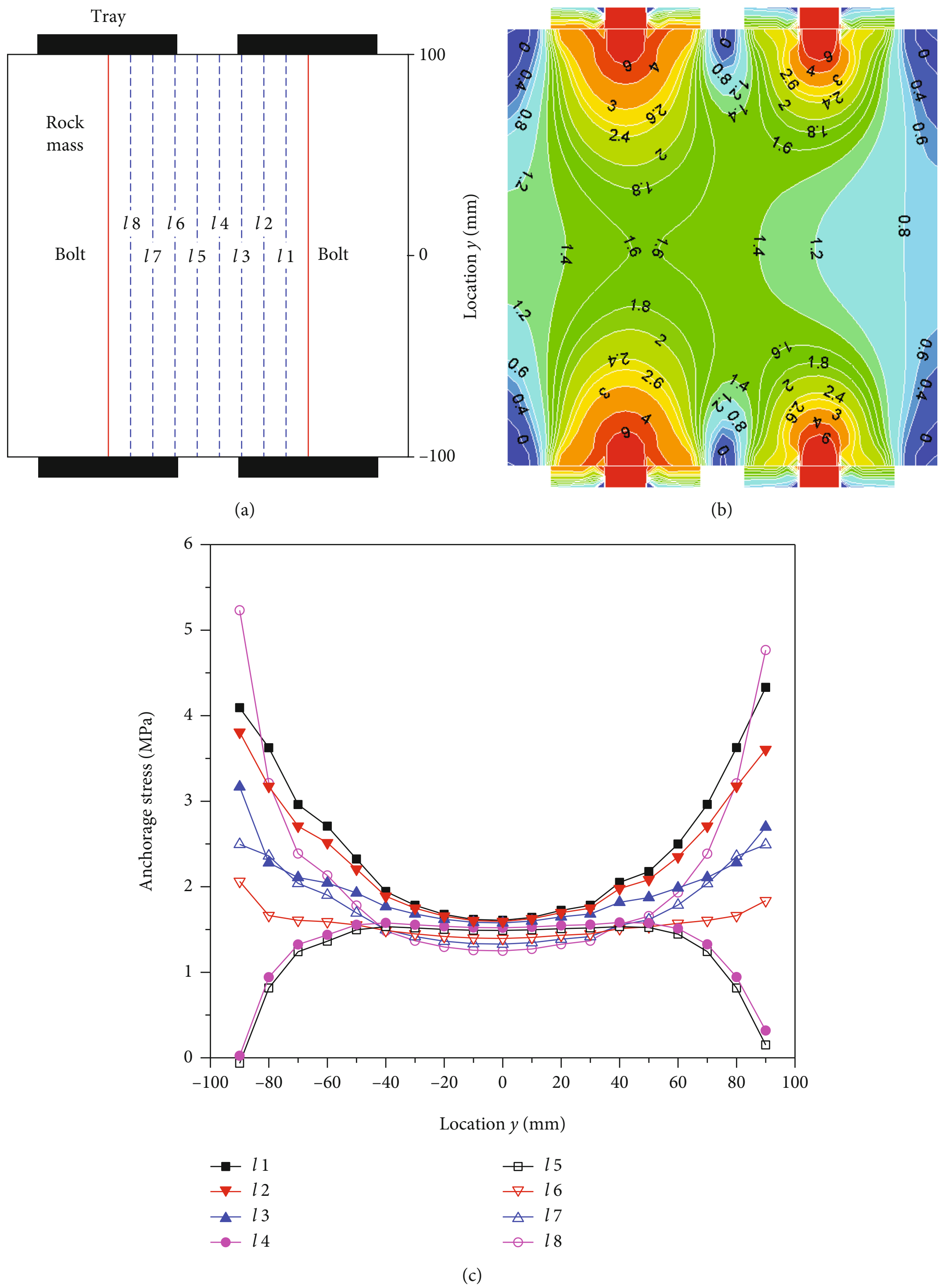

Figure 11: (a) Interested section and line, (b) anchorage stress distribution of interested section of rock mass specimen with two bolts reinforced, and (c) anchorage stress distribution in the interested lines.

multibolt anchorage surrounding rock mass model, the side of the bolt facing the loading end also showed this clear inclined stress rise zone. The difference is that, for the multibolt anchorage surrounding rock mass model, in the z direction, the stress rise zone is also formed in the area between bolts. It is noteworthy that the opposite stress reduction zone is formed in the area between bolts in the x direction. The same is that, whether in the x direction or in the z direction, the maximum principal stress is relatively small in the vicinity of the bolt.

The bolt primarily enhances the mechanical properties of the anchorage rock mass through anchorage stress. Therefore, the stress field of bolt action is a key indicator for analyzing the effect of the bolt. The anchorage stress and the

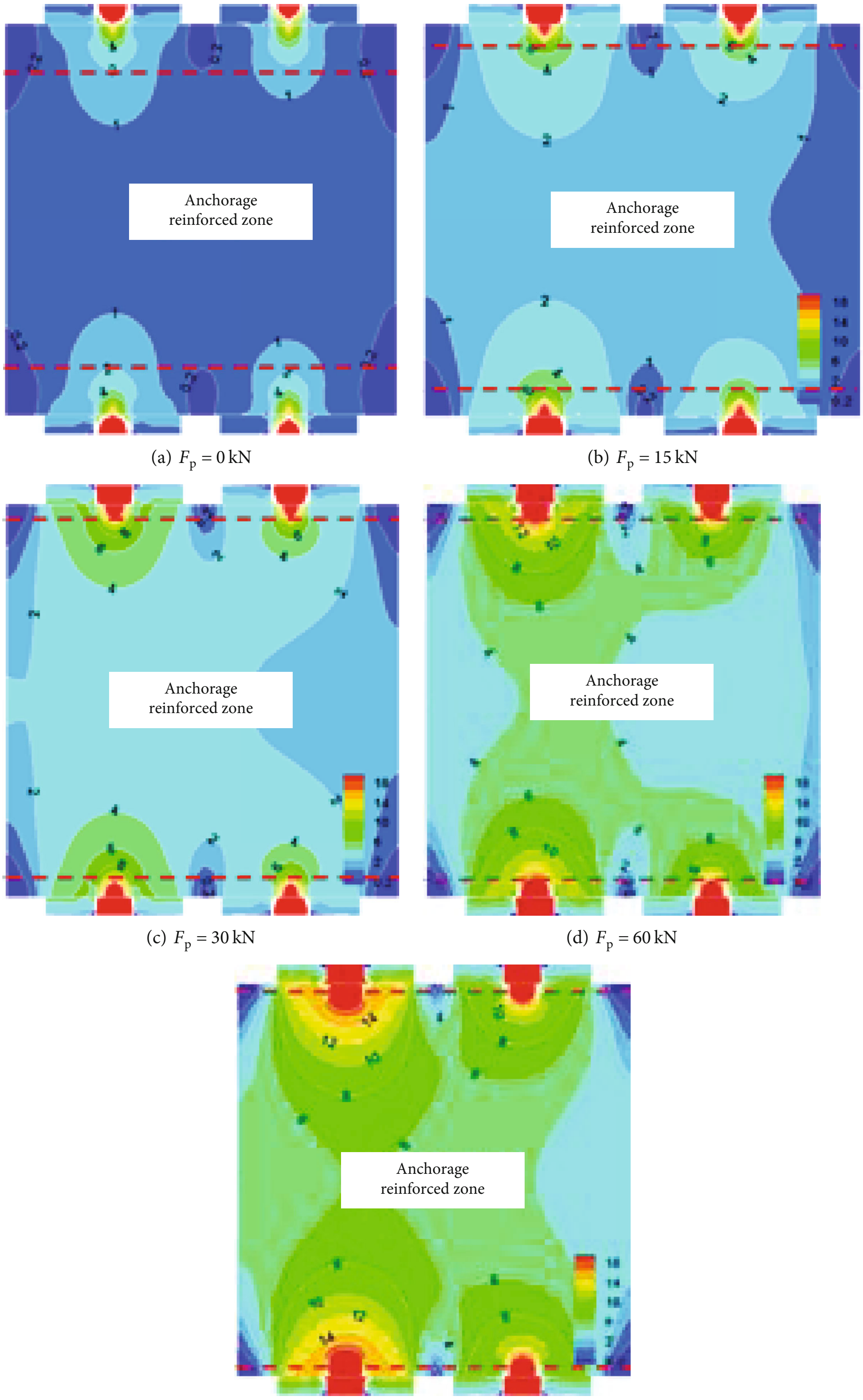

(a) $F_p = 0\,\text{kN}$ (b) $F_p = 15\,\text{kN}$ (c) $F_p = 30\,\text{kN}$ (d) $F_p = 60\,\text{kN}$ (e) $F_p = 90\,\text{kN}$

Figure 12: Anchorage stress distribution of rock mass specimen with different pretightening forces.

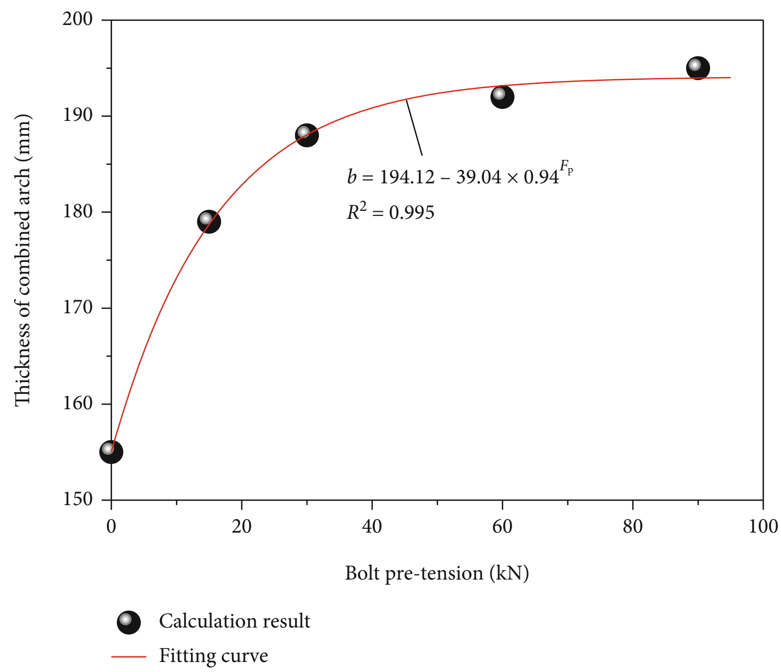

Figure 13: Effect of pretightening force on the thickness of combined arch.

distribution range of the anchorage stress in the anchorage model rise dramatically when the bolt number increases, as shown in Figure 8. In other words, the anchorage model's mechanical characteristics continue to rise as the bolt density rises. Furthermore, the anchorage stress between bolts of the multibolt anchorage surrounding rock mass model significantly decreases in the x direction.

3.3. Influence of Lateral Pressure on the Mechanical Behaviors of Rock Mass. Affected by the geological tectonic movement, the distribution laws of ground stress are complicated and changeable, and high-level tectonic stress exists in some regions. Therefore, a variety of model tests with varied lateral pressures (0 MPa, 0.5 MPa, 1.5 MPa, 3 MPa, 6 MPa, and 9 MPa) were carried out, and the effect of lateral pressure on the mechanical properties of the anchorage model and internal stress distribution was studied. The relationship between the peak strength and varied lateral pressures in the anchorage surrounding rock mass model is shown in Figure 9. As the lateral pressure level rises, the peak strength of the model shows a gradual increasing trend, but the reduction extent gradually decreases. When the lateral pressure level changes from 0 MPa to 3 MPa, the peak strength of the model increases dramatically. However, when the lateral pressure is greater than 3 MPa, the peak strength of the model rises slowly with the increase in the lateral pressure. The nonlinear relationship between the axial peak strength and the lateral pressure in the anchorage model is obtained by nonlinear fitting. As shown in Figure 9, the fitting results are accurate, which can provide a useful basis for future research.

Four lateral pressure conditions were designed in this experiment to investigate the impact rule of lateral pressure on the internal spatial stress distribution characteristics in the anchorage surrounding rock mass model: 0 MPa, 0.5 MPa, 1.5 MPa, and 6 MPa. Two mutually perpendicular planes were chosen as monitoring planes for the model in each working state. The maximum principal stress and the anchorage stress distributions on the monitoring plane for each working state under the peak strength are shown in Figure 10. The maximum principal stress around the bolt is relatively low for the anchorage rock mass model without lateral pressure. The stress in the middle part of the bolt rises in the model, and the size of this region grows gradually as the lateral pressure increases. The area with large stress expands in the x direction as the lateral pressure increases, from the central area where anchorage stress increases to the two ends where lateral pressure is applied. From the loading end to the bolt region, an obvious stress concentration zone exists in the z direction, and the stress concentration zone grows as the confining pressure rises. The anchorage stress and the maximum principal stress have similar distribution characteristics: the anchorage stress is higher in the vicinity of the bolt, and the area connected between the bolt and the tray has a noticeable stress increase zone. The area of the stress field around the bolt in the peak period gets bigger as the lateral pressure increases.

4. Discussion

According to previous research, the stress field analysis of the bolting support is an important tool for understanding bolt action processes. The peak states of anchorage models with two bolts were chosen to explore the variation law of the anchorage stress field (*syy*) in the anchorage rock mass model quantitatively, as shown in Figure 11. Considering the symmetry, the monitoring plane was chosen to be in the center of the model (over the coordinate origin, vertical

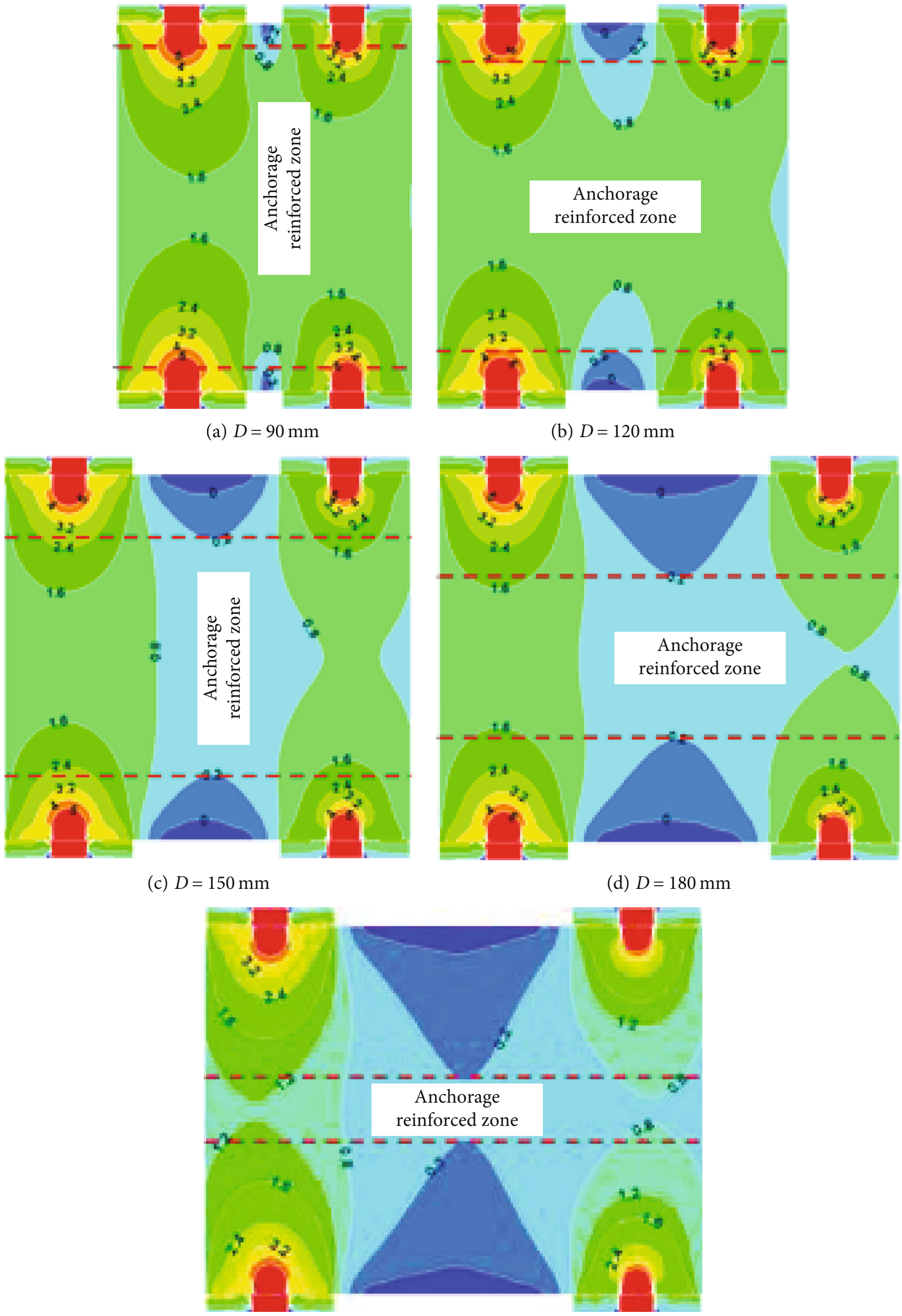

(a) $D = 90$ mm (b) $D = 120$ mm

(c) $D = 150$ mm (d) $D = 180$ mm

(e) $D = 200$ mm

Figure 14: Anchorage stress distribution of rock mass specimen with different bolt spacings.

z axis, and in the same plane as the bolt), as illustrated in Figure 11(a). Eight monitoring lines ($l1$~$l8$) were uniformly distributed across the middle plane of two bolts, with 19 monitoring points spread on each monitoring line. As illustrated in Figure 11(b), the area connected between the bolt and the tray has a noticeable stress concentration zone of the anchorage stress. The anchorage stress decreases slowly along its route, whereas the anchorage stress perpendicular to the bolt's direction decreases rapidly. The changing law of *syy* stress on the monitoring line in the axial direction

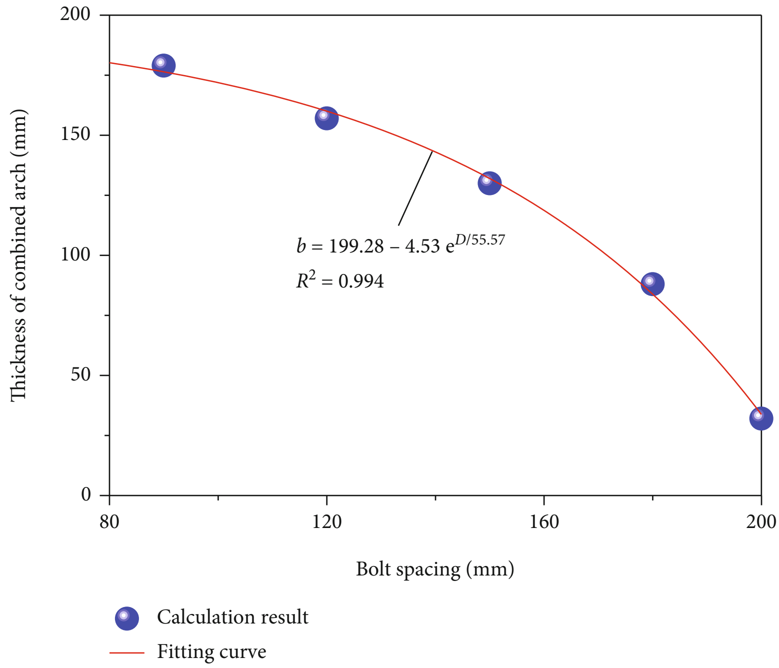

Figure 15: Effect of bolt spacing on the thickness of combined arch.

of the bolt at peak state is depicted in Figure 11(c). When the monitoring line is close to the bolt ($l1$~$l3$ and $l6$~$l8$), the *syy* stress of the monitoring points changes from dropping to increasing in the direction of the bolt. However, the *syy* stress on the monitoring lines $l4$ and $l5$ displays the change characteristics of a "crest shape" with a symmetrical increase from both ends to the middle.

According to the composite arch theory [33, 34], a single bolt can squeeze the surrounding rock and create a conical compression zone on both sides of the bolt under pretightening force. When the bolts are suitably spaced, the compression zones formed by each individual bolt can be layered on top of one another, resulting in a homogeneous compression zone of a definite thickness. Bolt reinforcement forms a combined reinforcement arch with a defined thickness around the roadway. The arch has a high bearing capacity and compressibility, allowing it to sustain the roadway well. The thickness of a rock-soil anchored composite arch is frequently linked to the bolting support parameters, according to a substantial quantity of study expertise. Therefore, the numerical simulation method was utilized to investigate the stress distribution in the anchorage rock mass and its influence on the thickness of the composite arch under different pretightening forces and bolt row spacings.

Figure 12 shows the distribution of the internal anchorage stress field in the model with five different pretightening forces (0, 15, 30, 60, and 90 kN). Based on the fluctuation of peak strength with lateral pressure in Section 3.3, the 0.2 MPa criteria were defined, implying that the anchorage area is recognized as the area where the anchorage stress is greater than 0.2 MPa. In the model, the anchorage stress field (middle symmetry plane) is shown under various pretightening forces. As the pretightening force increases, the anchorage strengthening area steadily rises, and the stress value in the anchorage strengthening region also climbs drastically. The axial force of the bolt causes the surrounding rock to convert from a uniaxial compression state before anchorage to a triaxial compression state. Thus, the lateral compressive strength of the surrounding rock is improved, and the rock is compacted and reinforced.

The variation of the thickness of the composite arch with the bolt pretightening force is obtained (in Figure 13). When the pretightening force rises from 0 kN to 15 kN, the thickness of the composite arch in the model increases from 155 mm to 179 mm, which is an increase of 15.48%. As the pretightening force changes from 15 kN to 30 kN, the thickness of the composite arch in the model changes from 179 mm to 188 mm, with a change extent of 5.03%. With the pretightening force raised from 30 kN to 60 kN, the thickness of the composite arch in the model increased by 2.13%, from 188 mm to 192 mm. When the pretightening force changes from 60 kN to 90 kN, the thickness of the composite arch in the model changes from 192 mm to 195 mm, which is increased by 1.56%. As the pretightening force increases, the thickness of the composite arch between bolts steadily increases. When the pretightening force exceeds 30 kN, the thickness of the composite arch is drastically reduced, indicating that there is a reasonable bolt pretightening force to achieve the required anchorage effect.

Figure 14 depicts the distribution of the internal anchorage stress field in the model for five different bolt row spacings (90, 120, 150, 180, and 200 mm). When the bolt row spacing is increased, the anchorage reinforcement area gradually shrinks, and the stress value in the anchorage reinforcement region also decreases considerably. Simultaneously, as the bolt row spacing rises, the area with insufficient anchorage stress between bolts grows, and the area has a conical symmetric distribution. As shown in Figure 15, the variation of the thickness of the composite arch with the bolt row spacing is obtained. When the bolt row spacing changes from 90 mm to 120 mm, the thickness of the composite arch in the model decreases from 179 mm to 157 mm, which is reduced by 12.29%. As the bolt row spacing rises from 120 mm to 150 mm, the thickness of the composite arch in the model changes from 157 mm to 130 mm, with a change extent of 17.20%. The thickness of the composite arch in the model reduces by 32.31%, from 130 mm to 88 mm, when the bolt row spacing changes from 150 mm to 180 mm. The thickness of the composite arch in the model decreases from 88 mm to 32 mm as the bolt row spacing increases from 180 mm to 200 mm, with a change extent of 63.64%. As the bolt row spacing is increased, the thickness of the composite arch between bolts steadily decreases. The anchorage strengthening area of bolts and the thickness of the composite arch are reduced when the bolt row spacing exceeds 150 mm, indicating that the recommended maximum bolt row spacing should be specified to enable efficient anchorage in actual engineering.

5. Conclusions

This work, which was based on the bolting support of roadway surrounding rock at Gubei coal mine, simplified the sidewall region of the roadway's surrounding rock influenced by the bolt anchorage to the anchorage rock mass model. The mechanical properties (such as peak strength, the principal stress, and the anchorage stress) of the anchorage rock mass under various bolt numbers (bolt density) and lateral pressures were determined using laboratory compression tests and the FLAC3D numerical simulation tests. The impacts of pretightening force and bolt row spacing on the total anchorage effect of bolts were explored using the composite arch theory. The following are the primary conclusions:

(1) The internal anchorage stress field of the specimen shows the following law as a whole: the near-point anchorage stress in the end area of the bolt is large, and the far-point anchorage stress is small. The near-point anchorage stress is small, and the far-point anchorage stress is large in the middle area of bolt. As the number of bolts (bolt density) in the anchorage rock mass model grows, the anchorage stress and distribution range increase considerably. The fluctuation of the anchorage stress field at different distances can be decreased by increasing the bolt number (bolt density)

(2) The maximum principal stress field stress of the anchorage rock mass improves as lateral pressure increases, the coverage region with larger stress expands, and the anchorage stress field expands as well. The anchorage mechanical properties of the anchorage rock mass, on the other hand, tend to be stable when the lateral pressure level is greater than 3 MPa

(3) Increased pretightening force and decreased bolt row spacing can improve the coverage range of the anchorage stress field and the thickness of the anchorage rock mass composite arch within a reasonable range. Thus, the appropriate pretightening force and bolt row spacing can improve the mechanical properties of the anchorage rock mass, making it more stable

Data Availability

The data used to support the findings of this study are available from the corresponding author upon request.

Conflicts of Interest

The authors declare that they have no conflicts of interest.

Acknowledgments

This study is financed by the National Natural Science Foundation of China (no. 42077240).

References

[1] Y. X. Sun, "Research on the deformation mechanism of mining roadway stratiform surrounding rock with nonuniform stress field," *Shock and Vibration*, vol. 2021, Article ID 6624045, 19 pages, 2021.

[2] Y. L. Hai, G. W. Zhi, L. Ji, and B. Lang, "Coal seam roadway bolt support design method based on the supporting theory of broken rock zone," *Advanced Materials Research*, vol. 734-737, no. 734-737, pp. 535–539, 2013.

[3] G. Y. Guo, H. P. Kang, D. Y. Qian, F. Q. Gao, and Y. Wang, "Mechanism for controlling floor heave of mining roadways using reinforcing roof and sidewalls in underground coal mine," *Sustainability*, vol. 10, no. 5, p. 1413, 2018.

[4] C. X. Zhao, Y. M. Li, G. Liu, and X. R. Meng, "Mechanism analysis and control technology of surrounding rock failure in deep soft rock roadway," *Engineering Failure Analysis*, vol. 115, article 104611, 2020.

[5] S. S. Yu and J. Z. Li, "Pre-reinforcement technology in broken roof side condition," *Applied Mechanics and Materials*, vol. 215-216, no. 215-216, pp. 681–684, 2012.

[6] J. K. Xu, R. Zhou, D. Z. Song, N. Li, K. Zhang, and D. Y. Xi, "Deformation and damage dynamic characteristics of coal-rock materials in deep coal mines," *International Journal of Damage Mechanics*, vol. 28, no. 1, pp. 58–78, 2019.

[7] W. X. Zhu, H. W. Jing, L. J. Yang, B. Pan, and H. J. Su, "Strength and deformation behaviors of bedded rock mass under bolt reinforcement," *International Journal of Mining Science and Technology*, vol. 28, no. 4, pp. 593–599, 2018.

[8] S. X. Ding, H. W. Jing, K. F. Chen, G. A. Xu, and B. Meng, "Stress evolution and support mechanism of a bolt anchored in a rock mass with a weak interlayer," *International Journal of Mining Science and Technology*, vol. 27, no. 3, pp. 573–580, 2017.

[9] Y. L. Chen, J. Y. Teng, R. A. Bin Sadiq, and K. Zhang, "Experimental study of bolt-anchoring mechanism for bedded rock mass," *International Journal of Geomechanics*, vol. 20, no. 4, 2020.

[10] S. C. Li, H. T. Wang, Q. Wang et al., "Failure mechanism of bolting support and high-strength bolt-grouting technology

for deep and soft surrounding rock with high stress," *Journal of Central South University*, vol. 23, no. 2, pp. 440–448, 2016.

[11] Y. M. Zhao, N. Zhang, and X. G. Zheng, "Experimental study of axial stress distribution and transfer along the bolt rods in an underground coal mine," *Arabian Journal of Geosciences*, vol. 9, no. 1, 2016.

[12] B. Wang, X. X. Guo, H. Jin, F. H. Li, and Y. Song, "Experimental study on degradation behaviors of rock bolt under the coupled effect of stress and corrosion," *Construction and Building Materials*, vol. 214, pp. 37–48, 2019.

[13] W. L. Zhang, L. Huang, and C. H. Juang, "An analytical model for estimating the force and displacement of fully grouted rock bolts," *Computers and Geotechnics*, vol. 117, article 103222, 2020.

[14] C. H. Liu and Y. Z. Li, "Predicting the shear resistance contribution of passive fully grouted bolts to jointed rock," *International Journal of Geomechanics*, vol. 20, no. 2, article 04019174, 2020.

[15] S. L. Yang, M. Li, G. F. Song, Y. Yang, and F. Xie, "Optimization of face flexible bolting and grouting technology for longwall face support under difficult geological conditions," *Energy Science and Engineering*, vol. 8, no. 4, pp. 1260–1270, 2020.

[16] H. W. Jing, J. Y. Wu, Q. Yin, and K. Wang, "Deformation and failure characteristics of anchorage structure of surrounding rock in deep roadway," *International Journal of Mining Science and Technology*, vol. 30, no. 5, pp. 593–604, 2020.

[17] H. P. Kang, J. H. Yang, and X. Z. Meng, "Tests and analysis of mechanical behaviours of rock bolt components for China's coal mine roadways," *Journal of Rock Mechanics and Geotechnical Engineering*, vol. 7, no. 1, pp. 14–26, 2015.

[18] Y. Li, C. Li, L. Zhang, W. S. Zhu, S. C. Li, and J. Liu, "An experimental investigation on mechanical property and anchorage effect of bolted jointed rock mass," *Geosciences Journal*, vol. 21, no. 2, pp. 253–265, 2017.

[19] H. P. Kang, "Support technologies for deep and complex roadways in underground coal mines: a review," *Internal Journal of Coal Science and Technology*, vol. 1, no. 3, pp. 261–277, 2014.

[20] H. P. Kang, "Analysis on load bearing ring in surrounding rock of roadway," *Rock and Soil Mechanics*, vol. 17, no. 4, pp. 84–88, 1996, (In Chinese).

[21] C. Cao, N. Jan, T. Ren, and A. Naj, "A study of rock bolting failure modes," *International Journal of Mining Science and Technology*, vol. 23, no. 1, pp. 79–88, 2013.

[22] H. W. Song and B. S. Mu, "Research on load capability and rational thickness of a reinforced broken rock arch," *Journal of China University of Mining and Technology*, vol. 26, no. 2, pp. 33–35, 1997, (In Chinese).

[23] X. Q. Guo, X. B. Mao, C. Ma, and J. L. Huang, "Bolt support mechanism based on elastic theory," *International Journal of Mining Science and Technology*, vol. 23, no. 4, pp. 469–474, 2013.

[24] Y. D. Zhang, L. Cheng, and J. F. Yang, "Bearing characteristic of composite rock-bolt bearing structure under different bolt support density," *Journal of Mining and Safety Engineering*, vol. 32, no. 2, pp. 305–309, 2015, (In Chinese).

[25] Y. J. Zong, L. J. Han, Q. Tao, and S. Q. Yang, "Mechanical properties and failure characteristics of fractured sandstone with grouting and anchorage," *Mining Science and Technology*, vol. 24, no. 2, pp. 165–170, 2014.

[26] Z. Du, B. Qin, and F. Tian, "Numerical analysis of the effects of rock bolts on stress redistribution around a roadway," *International Journal of Mining Science and Technology*, vol. 26, no. 6, pp. 975–980, 2016.

[27] H. J. Su, H. W. Jing, H. H. Zhao, L. Y. Yu, and Y. C. Wang, "Strength degradation and anchoring behavior of rock mass in the fault fracture zone," *Environmental Earth Sciences*, vol. 76, no. 4, p. 179, 2017.

[28] Q. Yin, H. W. Jing, H. J. Su, and H. H. Zhao, "Experimental study on mechanical properties and anchorage performances of rock mass in the fault fracture zone," *International Journal of Geomechanics*, vol. 18, no. 7, article 04018067, 2018.

[29] Z. J. Zhang, Q. L. Han, S. W. Liu, and Y. M. Li, "Roof bolts broken mechanism and their reasonable construction structures," *Key Engineering Materials*, vol. 306-308, no. 1-2, pp. 37–42, 2006.

[30] J. C. Chang, K. He, D. D. Pang, D. Li, C. M. Li, and B. J. Sun, "Influence of anchorage length and pretension on the working resistance of rock bolt based on its tensile characteristics," *International Journal of Coal Science and Technology*, vol. 8, no. 6, pp. 1384–1399, 2021.

[31] T. G. Sitharam, V. B. Maji, and A. K. Verma, "Practical equivalent continuum model for simulation of jointed rock mass using FLAC3D," *International Journal of Geomechanics*, vol. 7, no. 5, pp. 389–395, 2007.

[32] H. Wang, Z. X. Chen, and D. M. Zhang, "Rock slope stability analysis based on $FLAC^{3D}$ numerical simulation," *Applied Mechanics and Materials*, vol. 170-173, pp. 375–379, 2012.

[33] W. Hoek and E. T. Brown, *Underground Excavations in Rock*, The Institution of Mining and Metallurgy, 1980.

[34] H. Y. Yang, Y. B. Liu, Y. Li et al., "Research on the support of larger broken gateway based on the combined arch theory," *Geomechanics and Engineering*, vol. 23, no. 2, pp. 93–102, 2020.